Earth Planet. Sci. Lett. 623 (2023) 118425

Contents lists available at ScienceDirect

Earth and Planetary Science Letters

journal homepage: www.elsevier.com/locate/epsl

Changes in groundwater dynamics and geochemical evolution induced by drainage reorganization: Evidence from ^{81}Kr and ^{36}Cl dating of geothermal water in the Weihe Basin of China

Jie Li [a], Zhonghe Pang [b,c,d,*], Yulian Liu [a], Shuiming Hu [e,f], Wei Jiang [e,f,*], Lijun Tian [g], Guomin Yang [e,f], Ying Jiang [a], Xuan Jiao [a], Jiao Tian [h]

[a] Engineering Research Center of Groundwater Pollution Control and Remediation, Ministry of Education, College of Water Sciences, Beijing Normal University, Beijing 100875, China
[b] Key Laboratory of Shale Gas and Geoengineering, Institute of Geology and Geophysics, Chinese Academy of Sciences, Beijing 100029, China
[c] Geothermal Research Center, Institute of Geology and Geophysics, Chinese Academy of Sciences, Beijing 100029, China
[d] University of Chinese Academy of Sciences, Beijing 100049, China
[e] Hefei National Laboratory, University of Science and Technology of China, Hefei, 230088, China
[f] Hefei National Research Center for Physical Sciences at the Microscale and School of Physical Sciences, University of Science and Technology of China, Hefei, 230026, Anhui, China
[g] Center for Agricultural Resources Research, Institute of Genetics and Developmental Biology, Chinese Academy of Sciences, Shijiazhuang 050022, China
[h] Key Laboratory of Earthquake Prediction, Institute of Earthquake Forecasting, China Earthquake Administration, Beijing 100036, China

ARTICLE INFO

Keywords:
^{81}Kr dating
^{36}Cl dating
Geothermal water
Groundwater dynamics
Weihe basin

ABSTRACT

^{81}Kr and ^{36}Cl can both be used to date groundwater beyond the dating range of ^{14}C. ^{81}Kr usually provides reliable groundwater ages because it has uniform initial distribution and negligible subsurface generation, while ^{36}Cl is commonly influenced by subsurface sources or "dead" chloride dissolution. Therefore, the combined use of ^{81}Kr and ^{36}Cl could provide clues on the evolution history of groundwater. In the present study, we performed ^{36}Cl and ^{81}Kr dating of geothermal water in Weihe Basin of China and interpreted the possible cause of disagreement. Two distinct water masses were identified with distinctive isotopic signals: groundwater with significant δ^{18}O shifts (up to −2.0‰), dissolved dead Cl and ages < 1.0 Ma (Cluster A), and older water with little δ^{18}O shifts, negligible dissolved Cl and ages >1.0 Ma (Cluster B). The results confirm the eastward flow path of Cluster B to the Ancient Sanmen Lake with an increasing trend of Cl concentration and age. Modern recharge from the mountains flows to the basin center with intense interaction between water and carbonate under respective reservoir temperatures (100 ~ 130 °C). These waters flow through the saline stratum emerging from the spillover of the Ancient Sanmen Lake, resulting in higher dead Cl dissolution. A significant linear relationship is observed with the older end-member of ~1.3Ma under the topographically-driven faster circulation effect. ^{81}Kr ages seem to support the hypothesis that the birth of the modern Yellow River was at about 1.0–1.3 Ma. We inferred the drainage reorganization from the Ancient Sanmen Lake to the modern Yellow River since the Mid-Pleistocene Transition induced the change in groundwater dynamics as well as its chemical evolution. The excavation of the Ancient Sanmen Lake and the accentuated incision of the Weihe River induced groundwater gradient, and therefore the recharge from precipitation from both slopes of the Qinling Mountains in the south and the Beishan Mountains in the north. Our results highlight the effects of dead Cl on ^{36}Cl dating and demonstrate the significant impact of catchment reorganization on groundwater dynamics and its chemistry.

1. Introduction

Groundwater flow systems and geochemical parameters are evolving in response to geological processes and climatic stresses, such as orogenic events and the buildup or demise of ice sheets (Alley et al., 2002). Denudation, for instance, contributed to the persistence of saline water in the shallow subsurface of the Appalachian Plateaus (Yager et al., 2017). Regional groundwater flow driven by topography flushed

* Corresponding authors.
E-mail addresses: z.pang@mail.iggcas.ac.cn (Z. Pang), wjiang1@ustc.edu.cn (W. Jiang).

https://doi.org/10.1016/j.epsl.2023.118425
Received 28 April 2023; Received in revised form 25 September 2023; Accepted 27 September 2023

ore-forming brines to distal margins of basins, such as the Western Canada sedimentary basin, North American tectonic belts, etc. (Garven, 1989; Bethke and Marshak, 1990). Multiple reversing flows in the deep Cambrian aquifer system of the Baltic Artesian Basin were induced by the expansion and demise of ice sheets over several glacial cycles (Gerber et al., 2017). Meanwhile, changes in groundwater dynamics may be accompanied by alterations of geochemical parameters resulting from diverse geochemical processes such as mixing and water-rock interaction (Clark and Friz, 1997; Li et al., 2023). Exploration, utilization, and conservation of groundwater resources heighten the need for a better understanding of groundwater flow systems and their geochemical evolution throughout geologic time.

Due to the difficulty in obtaining reliable groundwater residence times beyond the dating range of ^{14}C, our understanding of groundwater evolution in response to geological processes and climatic stresses is still limited. ^{36}Cl is a useful tracer for dating old groundwater due to its long half-life ($T_{1/2} = 301$ kyr). ^{36}Cl is a cosmogenic isotope produced in the atmosphere by cosmic-ray splitting of ^{40}Ar and neutron activation of

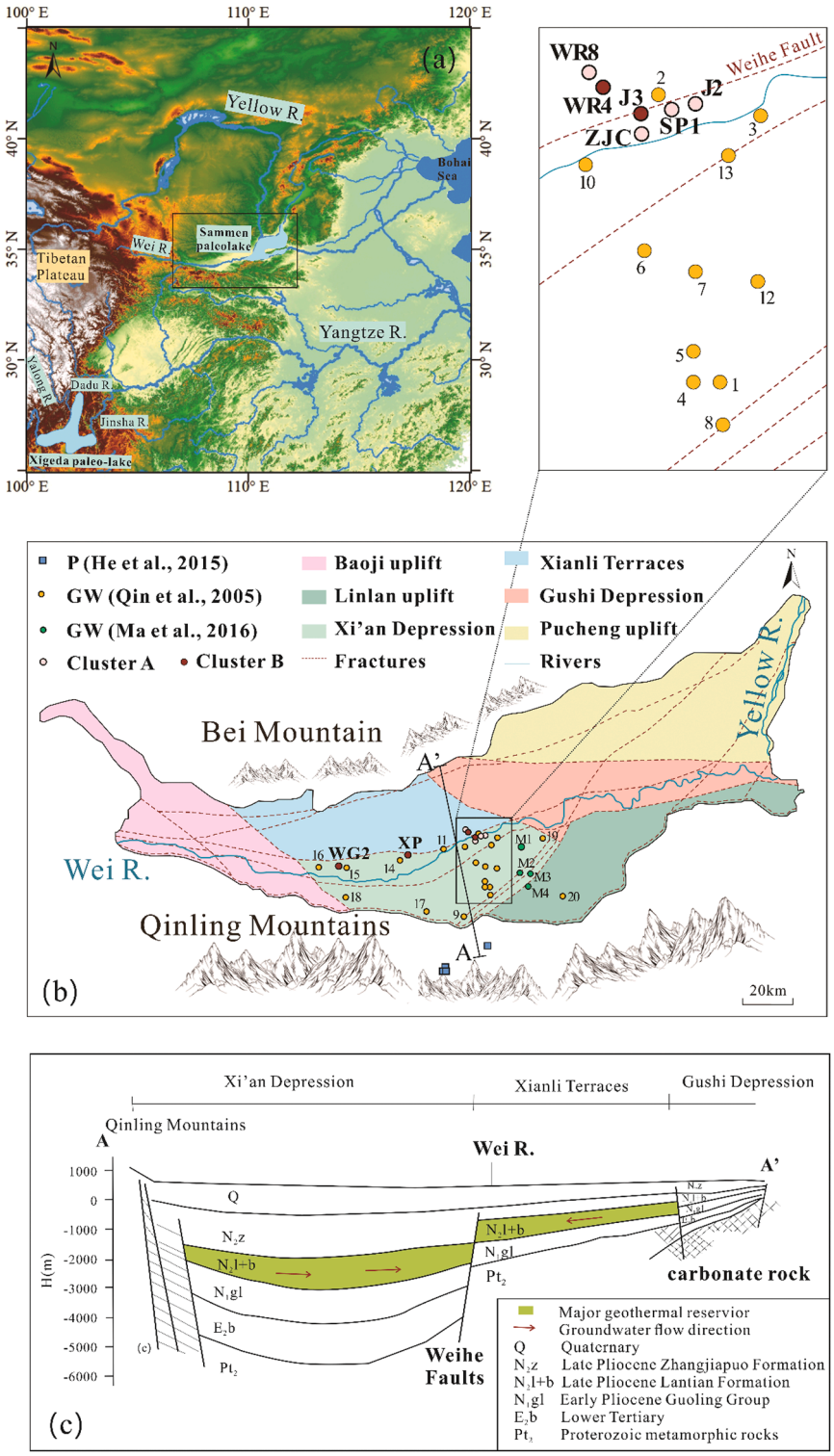

Fig. 1. The location of the Weihe Basin (a) and the sampling sites (b) with a schematic cross section A-A' (c).

^{36}Ar (Phillips, 2000). ^{36}Cl enters groundwater systems through wet deposition in the form of marine aerosols. In an ideal system (i.e., one with no subsurface sources of either ^{36}Cl or stable Cl and no sinks except for radioactive decay), calculating the ^{36}Cl model age is a simple matter of entering the initial and measured ^{36}Cl/Cl ratios into the radioactive decay equation and solving for the age (time). In actual aquifers, ^{36}Cl or stable Cl is often introduced in the subsurface through muon reactions and thermal neutron absorption. What's more, meteoric ^{36}Cl varies over time and space (Davis et al., 2003; Moysey et al., 2003). Due to the uncertainty of the initial content and potential underground sources of ^{36}Cl (Phillips, 2000; Park et al., 2002), the application of ^{36}Cl as a tracer to trace past groundwater flow fields is limited (Fehn et al., 1994; Patterson et al., 2005; Sherif et al., 2019). Therefore, it is valuable to calibrate the ^{36}Cl chronometers with other robust methods that are less or not affected by subsurface processes.

Recently, the development of atom trap trace analysis has made ^{81}Kr-dating available to groundwater research at large (Lu et al., 2014; Jiang et al., 2020). ^{81}Kr is chemically inert and a cosmogenic isotope with very limited subsurface production (Lehmann et al., 1993). Its atmospheric history is also relatively constant due to its long residence time in the air (Zappala et al., 2020). As a result, the interpretation of the ^{81}Kr data is straightforward (Jiang et al., 2012; Lu et al., 2014). Although this novel tracer has been used in quite a few groundwater studies recently (Lehmann et al., 2003; Sturchio et al., 2004; Matsumoto et al., 2018; Yechieli et al., 2019; Yokochi et al., 2019), few have investigated past groundwater dynamics and geochemical fields with effects of climatic or geological processes. ^{81}Kr dating of groundwater in the Baltic Artesian Basin in the range of 300 ka to >1.2 Ma revealed that it was comprised of three distinct fluid components, and the interface between precipitation and brines was impeded by Pleistocene glaciation (Gerber et al., 2017). The deep circulation of meteoric water in the Paradox Basin was strengthened by rapid denudation of the Colorado Plateau, as evidenced by ^{81}Kr groundwater age distributions (Kim et al., 2022). Due to the similar dating range of 5×10^4–10^6 yr for ^{81}Kr and ^{36}Cl, it is possible to calibrate the ^{36}Cl chronometers with ^{81}Kr and then enhance the use of ^{36}Cl data (Sturchio et al., 2004; Matsumoto et al., 2020). ^{81}Kr was applied to calibrate the input and the secular equilibrium ^{36}Cl/Cl values of ^{36}Cl chronometers for the first time in the Nubian Aquifer (Sturchio et al., 2004). Matsumoto et al. (2020) used ^{81}Kr to constrain the input values of ^{36}Cl/Cl and Cl in the deep Continental Intercalaire aquifer. Furthermore, the utilization of ^{81}Kr-calibrated-^{36}Cl dating offers a powerful tool, as it not only provides reliable residence time of the groundwater but also allows for the utilization of the isotopic abundances of ^{36}Cl as indicators to trace the sources of solutes for geochemical evaluation.

The Weihe Basin is located between the Qinling Mountains and the Beishan Mountains (Fig. 1), through which the Ancient Yellow River flowed before the formation of the Modern Yellow River with the major bends of the main river channel around the Ordos Block (Lin et al., 2001). Most geothermal water in the Weihe Basin is low in ^{14}C activity (<10 pmC) (Luo et al., 2017; Qin et al., 2005), approaching the dating limit of the ^{14}C method. Previous studies based on ^{36}Cl and ^{81}Kr tracers indicated that the mean residence time of the geothermal water is between a few hundred thousand and one million years (Ma et al., 2016; Li et al., 2017). The geothermal water in the Weihe Basin therefore offers an opportunity and a wealth of information that can be used to constrain the timing of the incision of the Sanmen Gorge and the birth of the Modern Yellow River, an issue still in academic debate, with ages ranging from the late Miocene to the late Pleistocene (Yang et al., 2009; Zhang et al., 2021; Wang et al., 2022).

Here we report a multi-tracer study based on ^{36}Cl and ^{81}Kr together with water chemistry of geothermal water in the deep aquifer, mainly the Lantian Formation of the Later Tertiary in the Weihe Basin. These tracers allow us to reveal the evolution of the groundwater flow system induced by catchment drainage changes, i.e., the excavation of the Ancient Sanmen Lake combined with the course change of the Yellow River. In addition, hydrogeological evidence is also incorporated to support the view that the Modern Yellow River originated at the beginning of the Mid-Pleistocene Transition (MPT, 1.25–0.7 Ma). Therefore, the age distribution and geochemical evolution of groundwater in the Weihe Basin provide strong evidence for the final integration of the Yellow River into its present form.

2. Study area

The Weihe Basin (33°00′N–35°20′N, 106°30′E–110°30′E) in Central China covers an area of 34,000 km^2 (Fig. 1), which is bounded to the north by the Bei Mountains and to the south by the Qinling Mountains. It contains approximately 7000 m of Cenozoic strata, filled predominantly with Tertiary fluvial and aeolian sediments, and Quaternary loess. Two main depressions, the Xi'an Depression and the Gushi Depression, are distributed throughout the basin. The Xianli Terrace is clamped to the north of the Xi'an Depression. The basement rock is Cenozoic granites and Proterozoic schist in the Xi'an Depression, and carbonate in the Xianli Terraces. There are abundant Cenozoic fractures and faults in the study area as shown in Fig. 1b, suggesting the Cenozoic extension in the study area (Mercier et al., 2013).

The Wei River runs through the study area and joins the Yellow River at Sanmen Gorge. Groundwater is recharged from the Ordos Basin in the north and the Qinling Mountains in the south (Fig. 1c) and discharged in the basin center (Li et al., 2017; Zhang et al., 2019). There are currently hundreds of wells drilled into Tertiary reservoirs between 1000 and 4000 m in depth for geothermal water exploitation. The late Pliocene Lantian formation consists mostly of bedded medium-grained feldspathic sandstone with interbeds of brown–red and silty mudstone, which is the main productive well section. Geothermal samples with measured δ^{11}B values between −8.8‰ and 12.5‰ confirmed the presence of halite from non-marine evaporites (He, 2015).

3. Data and methods

Water samples for major ions, stable isotopes (δ^2H and δ^{18}O), and radiochlorine (^{36}Cl) analysis were collected during the sampling campaign in 2016. A total of eight water samples were obtained from wells within the late Pliocene Lantian formation, with depths ranging from 2750 m to 3200 m. The major cation and anion concentrations were determined by ion chromatography at the Analytical Laboratory of the Beijing Research Institute of Uranium Geology. The charge balance error was less than ±5%, and the detection limit was 0.1 mg/L. δ^2H and δ^{18}O values were measured with a Picarro L1102-i water isotope analyzer at the Water Isotope and Water-Rock Interaction Laboratory, Institute of Geology and Geophysics, Chinese Academy of Sciences. The precisions for δ^2H and δ^{18}O were ±0.5‰ and ±0.1‰, respectively. ^{36}Cl samples were firstly prepared by AgCl precipitation and chromatographic purification, and then ^{36}Cl abundances, reported as ^{36}Cl/Cl in units of 10^{-15}, were measured by accelerator mass spectrometry (AMS) at the PRIME Laboratory of Purdue University.

^{36}Cl ages are generally calculated by the following equation, which considers the radioactive decay of ^{36}Cl and the in situ production of ^{36}Cl by thermal neutron capture (^{35}Cl(n, γ)^{36}Cl) within the aquifer (Bentley et al., 1986):

$$t = -\frac{1}{\lambda_{36}} \ln\left(\frac{R_m - R_{se}}{R_i - R_{se}}\right) \quad (1)$$

where λ_{36} is the ^{36}Cl decay constant (2.3×10^{-6} yr^{-1}) and R_m, R_{se} and R_i are the measured, secular equilibrium, and initial ^{36}Cl/Cl ratios, respectively. Generally, the subsurface ^{36}Cl/Cl of the aquifer is constant in secular equilibrium (R_{se}). In some cases, the dissolution of bedded evaporites and diffusion from stagnant, saline pore fluids in aquitards will bring new inputs; thus, a mass balance approach may be taken:

$$R_m C_m = \left[(R_i - R_{se})e^{-\lambda t} + R_{se}\right] \times C_i + R_{rk} C_{rk} \quad (2)$$

where R_{rk} is the $^{36}Cl/Cl$ ratio of the input to the aquifer. C_m and C_i are the measured and initial chloride concentrations, respectively. C_{rk} represents the Cl content added to the aquifer. The above equation can be rearranged and solved for time:

$$t = -\frac{1}{\lambda_{36}} \ln\left[\frac{1}{(R_i - R_{se})} \times \left(\frac{(R_m C_m - R_{rk} C_{rk})}{C_i} - R_{se}\right)\right] \quad (3)$$

The secular equilibrium ratio in a closed system is calculated with the following equation:

$$R_{se} = \frac{\Phi_n \chi_{35} \sigma_{35}}{\lambda_{36}} \quad (4)$$

where Φ_n is neutron flux, χ_{35} stands for the isotopic abundance of ^{35}Cl (0.75775), and σ_{35} is neutron capture cross-section (43.74×10^{-24} cm^2). Using the available data $\Phi_n = 2.0 \times 10^{-6}$ cm^{-2}·s^{-1} of the geothermal sandstone aquifer in the Weihe Basin (Ma et al., 2016), this expression yielded a secular equilibrium ratio of $(0.9 \pm 0.1) \times 10^{-15}$.

4. Results and discussion

4.1. Chloride sources

Chloride behaves conservatively in aquifers and does not go through adsorption or chemical reactions with aquifer materials. In order to trace the solute origin and physical processes such as mixing or evaporation, Cl^- concentrations together with H isotopic compositions for groundwater samples are shown in Fig. 2a. In the piedmont region of the Qinling Mountains, there are five precipitation samples with low Cl^-concentrations in the range of 0.8 to 4.3 mg/L. The eight geothermal water samples have Cl^-concentrations in the range of 1660 mg/L to 2960 mg/L, significantly higher than those of the precipitation but have similar δ^2H values. It is clear that the high Cl^- concentration is due to an external source of solutes, such as salt dissolutions. Additionally, the Cl^- concentrations in our geothermal water were also significantly higher than those of the non-thermal systems, such as the Continental Intercalaire aquifer (296–1188 mg/L) and the Nubian Aquifer (20–200 mg/L) (Matsumoto et al., 2020; Sturchio et al., 2004).

Measured $^{36}Cl/Cl$ ratios versus Cl^- concentrations (mg/L) are

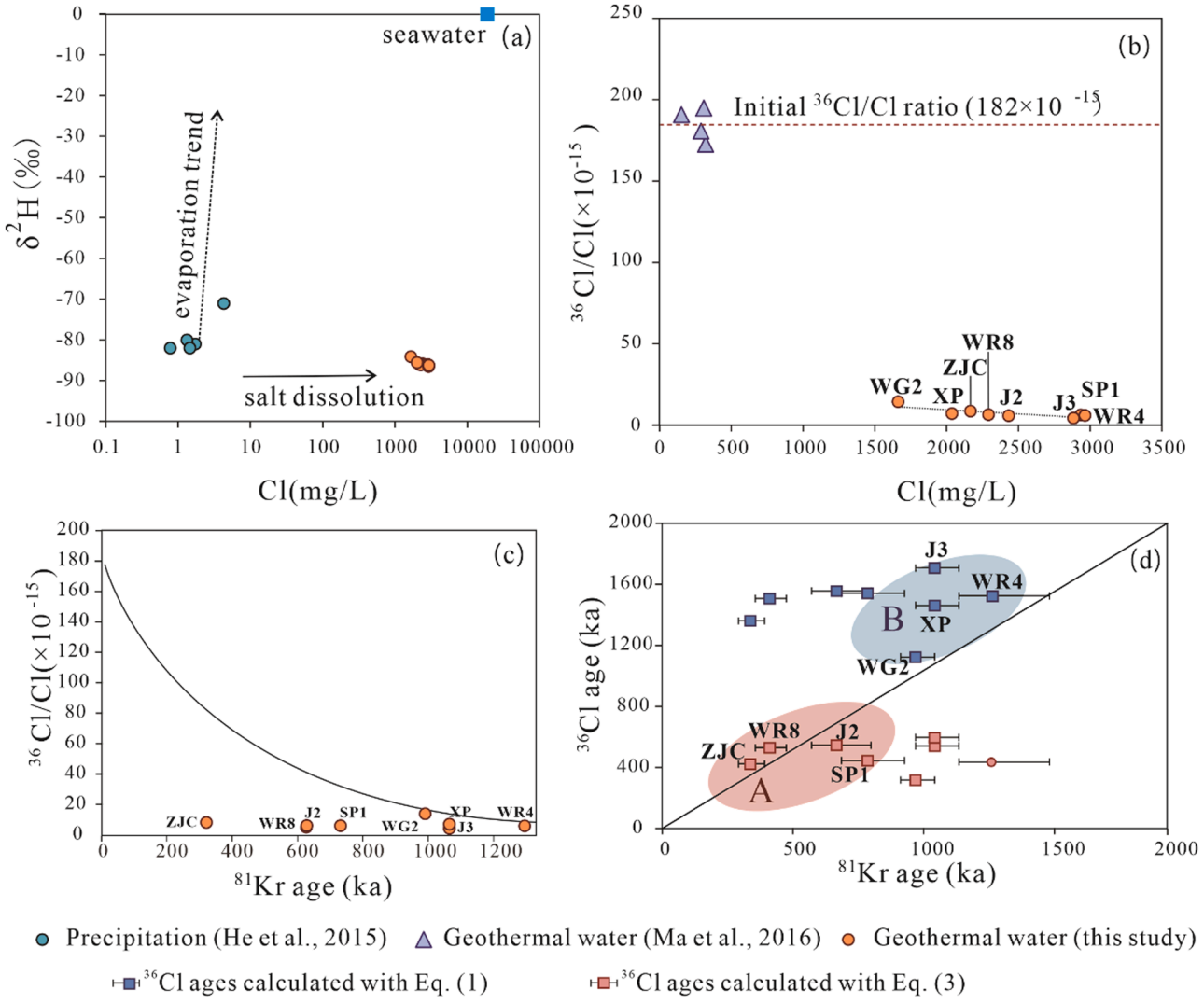

Fig. 2. Relationships between chloride concentrations and isotopic data. (a) δ^2H vs. Cl concentration (mg/L) in geothermal waters (red circles) and precipitation (blue circles, He, 2015). The seawater (blue solid square, Sherif et al., 2019) and the evaporation trend calculated by the theoretical formula (Supplementary Materials) are also presented. (b) $^{36}Cl/Cl$ ratios vs. Cl concentration (mg/L) for the geothermal wells of the study area. The dashed red line indicated the assumed initial $^{36}Cl/Cl$ ratio in the study area. (c) $^{36}Cl/Cl$ ratios vs. the ^{81}Kr ages. The line is the $^{36}Cl/Cl$ ratios against ages calculated by Eq. (1) with the initial $^{36}Cl/Cl$ ratio of 182×10^{-15}, where the calculated ^{36}Cl age is assumed to be the same as the ^{81}Kr age. (d) ^{36}Cl ages vs. ^{81}Kr ages. The blue and red points are samples with ^{36}Cl ages calculated by Eq. (1) and Eq. (3), respectively.

presented in Fig. 2b for geothermal samples. Groundwaters from the geothermal system have $^{36}Cl/Cl$ ratios ranging from 4.3×10^{-15} to 14.2×10^{-15} (Table S1). In general, lower ratios are observed in the geothermal aquifers, implying longer residence times in the geothermal system. However, the effects of additional salt dissolution need to be taken into account in order to get the proper ^{36}Cl ages.

4.2. ^{36}Cl ages

Four geothermal samples in the southern area from Ma et al. (2016) have high $^{36}Cl/Cl$ values (170×10^{-15}–188×10^{-15}) (Fig. 2b). The average $^{36}Cl/Cl$ value of the geothermal samples is 182×10^{-15}, which is quite close to the initial ratio $Ri = 190 \times 10^{-15}$ estimated by Ma et al. (2016) with the theoretical natural ^{36}Cl fallout rate. Therefore, the initial $^{36}Cl/Cl$ is assumed to be 182×10^{-15}, and the average Cl^- concentration (268 mg/L) was assumed as the initial Cl^- concentration (C_i). The initial $^{36}Cl/Cl$ value was higher than the value previously found in the desert of Egypt (130×10^{-15} for Western Desert, Patterson et al., 2005; 90×10^{-15} for Eastern Desert, Sherif et al., 2019), but lower than those for the Continental Intercalaire aquifer in the Northern Tunisian Sahara (340 ~820 $\times 10^{-15}$, Matsumoto et al., 2020). A secular equilibrium ratio of 0.9×10^{-15} was obtained with the available data for the sandstone aquifer using Eq. (4). This obtained value was smaller than 8×10^{-15} for the Nubian sandstone reservoir in Egypt (Phillips, 2013; Sturchio et al., 2004) and 5×10^{-15} for the same aquifer (Patterson et al., 2005; Sherif et al., 2019). The reason for the difference of an order of magnitude may be attributed to the U and Th contents from the rock matrix in our aquifer. The average measured values of U and Th concentrations of the sandstone were 2.9 μg/g and 7.1 μg/g (Ma et al., 2016).

Fig. 2c presents $^{36}Cl/Cl$ ratios with the previously published ^{81}Kr ages (Li et al., 2017) in eight samples for which both measurements were made in the study area. The $^{36}Cl/Cl$ ratios were calculated with Eq. (1) (assuming an initial $^{36}Cl/Cl$ value of 182×10^{-15}), as shown by the curve in Fig. 2c. Four out of the 8 samples (ZJC, WR8, J2, and SP1) lie below the curve, which is an indication of influence due to the dissolution of "dead" chloride. The dead chloride may originate from evaporites with negligible U and Th (Bentley et al., 1986). Similar behavior has been reported in deep groundwater samples from the Northern Tunisian Sahara, where the deviation of the $^{36}Cl/Cl$ ratios from the decay curve was attributed to the dissolution of chloride within the aquifer (Matsumoto et al., 2020). However, the effect of "dead" chloride in our study played a more important role in the variation of the $^{36}Cl/Cl$ ratio of geothermal water. The reservoir temperatures are determined to be about 100 °C using a chemical geothermometer for the Tertiary reservoirs in the study area (see Supplementary Materials). As a result, more "dead" chloride can be dissolved.

To correct the effect of "dead" chloride, groundwater ^{36}Cl model ages were calculated using Eq. (3). In the calculation, R_{rk} is assumed to be 0 and $R_{se} = 0.9 \times 10^{-15}$. Both the uncorrected ^{36}Cl and corrected ^{36}Cl ages are plotted against the ^{81}Kr ages in Fig. 2d. First, we noticed that the corrected groundwater ^{36}Cl ages (from 314 to 593 kyr, Table S1, red points in Fig. 2d) were significantly smaller than the ^{36}Cl ages with no "dead" chloride correction calculated using Eq. (1) (from 1121 to 1705 kyr, blue points in Fig. 2d). The second thing worth noting is that the 8 samples clustered into two groups (denoted Cluster A and B in Fig. 2d). In Cluster B (WG2, XP, J3, and WR4), the uncorrected ^{36}Cl ages already agreed with the ^{81}Kr ages within measurement uncertainties, while the correction for dead chloride only made the ^{36}Cl ages and ^{81}Kr ages mismatch. But in Cluster A (ZJC, WR8, J2, and SP1), the dead chloride corrections were necessary to make the ^{36}Cl ages match with the ^{81}Kr ages. The classification of these two groups is supported by additional evidence from stable isotope and water chemistry data, which are presented in the next section.

4.3. Stable isotopes and recharge dynamics

The stable isotope compositions of the water samples are shown in Fig. 3a. The δ^2H values for the eight geothermal water samples are similar, between −84.1‰ and −86.5‰, while the $\delta^{18}O$ values are more variable, between −9.8‰ and −2.1‰. The samples exhibit positive $\delta^{18}O$ shifts from the GMWL, which were also found in previous studies (Qin et al., 2005; Luo et al., 2019). Generally, a positive $\delta^{18}O$ shift can be caused by one of the flowing factors or jointly: (1) the exchange of oxygen isotopes between carbonates and geothermal water at relatively low temperatures during a long residence time or (2) the exchange of oxygen isotopes between silicate minerals and geothermal water at high reservoir temperatures (> 250 °C) (Horita, 2005). The estimated reservoir temperature determined with Na-K-Mg chemical geothermometer (Giggenbach, 1988) and the method of Pang and Reed (1998) for the Tertiary reservoirs (Qin et al., 2005, and Supplementary Materials) in the study area was 100 ~ 130 °C, indicating the temperature of the reservoir when the water-rock equilibrium was reached. Therefore, the $\delta^{18}O$ shifts may have involved carbonates (Qin et al., 2005; Luo et al., 2019). Although there are similar reservoir temperatures for eight samples in the study area, the degree of $\delta^{18}O$ shifts varies among them. Smaller $\delta^{18}O$ shifts were observed in Cluster B, compared to those of Cluster A with the minimum $\delta^{18}O$ shift in the well WG2 (Fig. 3a and b). More interestingly, there is a negative correlation between $\delta^{18}O$ and ^{81}Kr ages (or a positive correlation between $\delta^{18}O$ and the isotopic abundance of ^{81}Kr, Fig. 3b), which is opposite to the trend for larger $\delta^{18}O$ shifts with longer water-rock interactions. We attribute the cause of this phenomenon to a binary mixing between a younger endmember (~350 ka, ZJC in Cluster A) with more positive $\delta^{18}O$ values around −2.1‰ and an older endmember (~1.3 Ma, J3 and WR4 in Cluster B) with more negative $\delta^{18}O$ values.

The younger endmember is characterized by a noticeable $\delta^{18}O$ shift of −2.1‰, which is due to the water-rock interaction between the groundwater and the surrounding carbonate. There is a good positive correlation between the wellhead temperature and $\delta^{18}O$ values of samples from Cluster A and most sites from Qin et al. (2005) (Fig. 3c), which is in agreement with the groundwater flow path in a northward direction. ^{14}C contents of these samples in the Xi'an Depression collected by Qin et al. (2005) decrease from 50.5 to 1.3 pmC, with an increasing trend of $\delta^{13}C$ in the dissolved inorganic carbon (Table S2), indicating the dissolution processes of carbonate minerals. The carbonate nodules in the Tertiary loess sediment have $\delta^{18}O$ values of −11.8‰ ~ −8‰ VPDB (Ding and Yang, 2000), which is the dominant ^{18}O source for the water-rock exchanges. Therefore, this end member is derived from modern recharge. The quick infiltration through deep faults in the mountain front of the Qinling Mountains and the high thermal background enhanced the dissolution processes of carbonate minerals. The wellhead temperature increases with the upward trend of $\delta^{18}O$ shifts and the increase of Cl concentrations along the flow direction (Fig. 3c and d).

A closer look at the relations between Cl concentrations and $\delta^{18}O$ further revealed an interesting and complex evolution history of Cluster A. First, the Cluster A samples showed large positive $\delta^{18}O$ shifts (−4‰ ~ −2‰). These values are close to the highest $\delta^{18}O$ shifts observed in Cluster C from Qin et al. (2005) (Fig. 3d). Second, compared to the data from Cluster C, the Cluster A samples have much higher Cl concentrations (an order of magnitude higher). Dead chloride dissolution of Cluster C (Fig. 3d) has been excluded due to low Cl concentrations (152 mg/L ~ 321 mg/L) and high ^{36}Cl data ($170 \times 10^{-15} \sim 192 \times 10^{-15}$, Ma et al. 2016) (see detailed discussions in the previous paragraph). Moreover, the groundwater ages of Cluster A (based on ^{81}Kr) are much older than the groundwater ages (based on ^{14}C) of Cluster C by Qin et al. (2005). Lastly, the distribution of Cluster A samples on the Cl - $\delta^{18}O$ plot (Fig. 3d) suggested a mixing between them and the old end member (WR4 and J3) in Cluster B. Based on this evidence and the discussion in the previous paragraph, we deduced that the water first went through

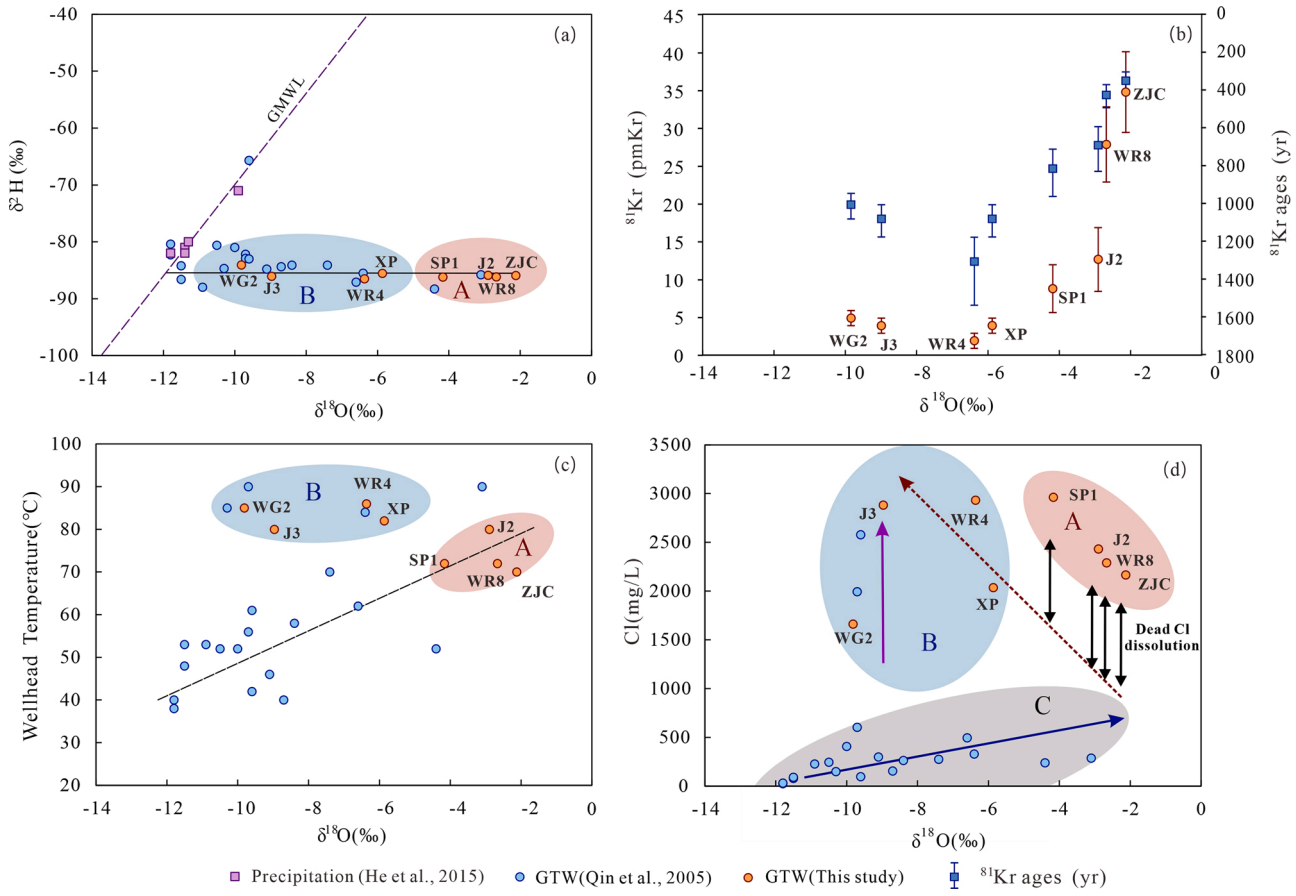

Fig. 3. (a) δ^2H (b) ^{81}Kr isotopic abundance and ages (c)wellhead temperature (℃) and (d) Cl concentration (mg/L) plotted against δ^{18}O of the thermal water samples (GMWL = global meteoric water line).

water-rock interaction with the carbonates and became ^{18}O enriched (blue arrows in Fig. 3d). Then they went through a dead chloride dissolution process as they mixed with an old end member. The dead chloride dissolutions cause the data to be shifted upward from the mixing line (red dotted line in Fig. 3d). We deduced that the mixing mainly occurs with the old water from WR4 and J3, as geographically WG2 and XP are located far from other samples (in the west of the study area, Fig. 1). This picture is also consistent with the binary mixing process in the ^{81}Kr-δ^{18}O plot in Fig. 3b. This analysis showed that only Cluster A was affected by the dead chloride dissolution, while Cluster B was not. This explains why the dead chloride correction had made the mismatches between the ^{36}Cl ages and ^{81}Kr ages smaller for Cluster A, but did not work for Cluster B in Section 4.2.

4.4. *Implication for drainage reorganization of the Yellow River catchment*

In this section, we discuss the implication of the geochemical data (^{81}Kr, ^{36}Cl, stable isotopes, water chemistry, wellhead temperature, etc.) and its linkage to a major geological event in the evolution history of Yellow River, i.e., the reorganization of Yellow River.

First, we resolve subsurface mixing and identify two distinct end-members: one high-salinity brine groundwater (δ^{18}O ≈ −10‰, 1.5~5.0 (g Cl)/L, >1.0Ma) discharged to the Ancient Sanmen Lake, and the other more recent (~350ka) recharge from both the Qinling Mountains and Bei Mountains with a north-south groundwater movement. This change in groundwater dynamics can be related to the excavation of Ancient Sanmen Lake and the drainage reorganization of the Modern Yellow River.

In the southern end of the piedmont area of the Qinling Mountains (Latitude of 34.16° to 34.34°, approximately 20 km), ^{14}C ages indicated a northward flow of ~2 m/yr (Qin et al., 2005). Further north, the distance from the Qinling Mountains to the basin center is approximately 40 km, and the flow rates suggested by the youngest ^{81}Kr ages (0.35 Ma) were about 0.1 m/yr. This decrease in flow rate toward the retention area indicates a decrease in hydraulic gradient and/or permeability. The youngest groundwater (WG2) from Cluster B has a ^{81}Kr age of 1.0 ± 0.1 Ma, which indicates that groundwater was generally recharged at around 1.0 Ma. The older ^{81}Kr ages (1.1 ± 0.1 Ma for XP, 1.1 ± 0.1 Ma for J3, and 1.3 ± 0.2 Ma for WR4) refer to the migration time from the west to the east. This trend is consistent with the geochemical evolution trend, i.e., the Cl^- concentration increases from the west (WG2, XP) to the east (WR4, J3) (see Figs. 3d and S1). This is due to the old groundwater discharged to the Ancient Sanmen Lake, located just in the east of the Weihe Basin (Fig. 4a). As shown in Fig. 3b, J3 and WR4 samples are deemed to be an old endmember with ages ~1.3 Ma for the linear mixing with younger groundwater (ZJC in Cluster A). XP is located on the red dotted line in Fig. 3d, showing a straight mixing between modern recharge (the rightmost blue point with a δ^{18}O of −3.1‰ in Fig. 3d) and old groundwater (J3 and WR4). The agreement between ^{81}Kr ages and ^{36}Cl ages without dead Cl dissolution for XP (Fig. 2d) indicates the absence of paleo-salt lake sedimentation here. The different properties and ages of groundwater in Cluster A and Cluster B indicate that the recharge dynamics had changed significantly in the past and provide insights to the birth time of the Modern Yellow River.

Previous studies suggested two major phases in the evolution of the Yellow River, the proto-Yellow River and the Modern Yellow River. There is a vast difference between flow patterns and dynamics of these two phases (Fig. 4a and b). The Paleo-Yellow River phase is marked by the existence of the Ancient Sanmen Lake, while the incision of the

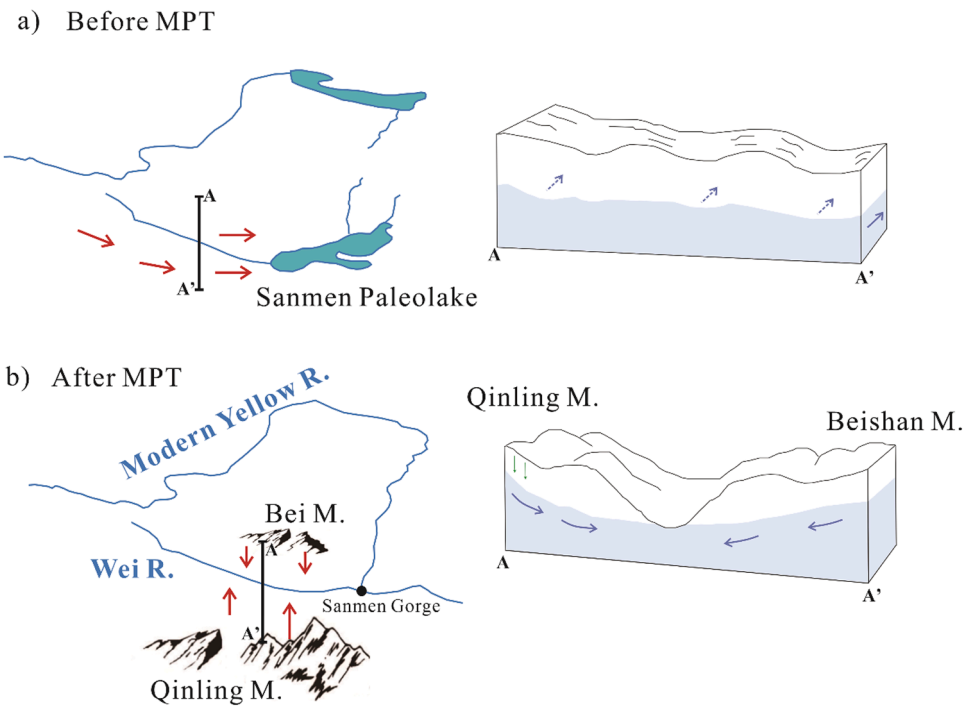

Fig. 4. Schematic diagrams of groundwater evolution in response to the drainage reorganization of the modern Yellow River a) before and b) after the Mid-Pleistocene Transition. Red arrows indicate groundwater flow directions.

Sanmen Gorge and spillover of the Ancient Sanmen Lake mark the birth of the Modern Yellow River. Several researchers estimated the birth time of the modern Yellow River was between 1.3Ma and 1.0 Ma (Kong et al., 2014; Hu et al., 2019; Liu et al., 2022; Wang et al., 2022). A continuous sedimentary archive from the SMX19 drill core in the Sanmen Basin (Wang et al., 2022), indicates that the modern Yellow River finally integrated at 1.25 Ma, similar to the beginning of the MPT. Furthermore, the evidence from detrital zircon U-Pb ages and heavy mineral assemblages as provenance tracers (Kong et al., 2014; Liu et al., 2022) also supports this view. The highest (oldest) terraces of the Yellow River in the Jinshaan Gorge and the Kouma region were developed at ~1.2 Ma, indicating that the connection between the middle and lower reaches of the Yellow River occurred no later than 1.2 Ma (Pan et al., 2005; Hu et al., 2019).

Our study on the thermal groundwater in the Weihe Basin provides additional information about the evolution history of the Yellow River and suggests the birth time of the modern Yellow River is about 1.0~1.3 Ma. First, the groundwater age of 1.0 ± 0.1 Ma for WG2 from Cluster B indicates the minimal extinction time of Ancient Sanmen Lake. Although WR4 and J3 are located very close to Cluster A, the absence of paleo-salt lake sedimentation of WR4 and J3 may suggest the oldest limit for the existence time of the Ancient Sanmen Lake at approximately 1.1–1.3 Ma. The dead Cl dissolution process in Cluster A likely originated from paleo-salt lakes, which could be linked to the spillover of Ancient Sanmen Lake. The oldest ^{81}Kr age of Cluster A (SP1) is approximately 0.81 Ma, much younger than the extinction time of the Ancient Sanmen Lake (1.0–1.3 Ma). The southward groundwater flow direction was confirmed with evidence from wellhead temperature, Cl concentrations, and δ^{18}O shifts (Fig. 3). δ^{18}O shifts become greater with the buildup of salinity after the recharge from the Mountains. Subsequently, dead Cl dissolution was triggered when groundwater flowed into the saline stratum, corresponding to the disappearance of Ancient Sanmen Lake. The cause of groundwater recharge on both sides, from the Qinling Mountains in the south and the Bei Mountains in the north, could be the incision of the Wei River or the quick uplift of the Qingling Mountains, which can both enhance groundwater head gradients. The intermittent uplift of the Qinling Mountains with an increasing trend of uplift speed was deduced since 10 Ma (Liu et al., 2013; Meng, 2017), corresponding to the uplift of the Northern Tibet Platea during 15 to 7 Ma with evidence from pollen records of montane conifers (Miao et al., 2022). Groundwater ages in Cluster A are in the range of 0.35–0.81 Ma, smaller than the uplift time by one order of magnitude, which suggests topographical uplift did not make enough head gradients until 0.35–0.81 Ma and required further accelerating process to enhance the head gradients to change groundwater dynamics in the Weihe Basin. This is confirmed by the study by Kim et al. (2022) in the Paradox Basin. According to that study, although the denudation of the Colorado Plateau began at 4–10 Ma (Lazear et al., 2013; Murray et al., 2019), it was insufficient to enhance regional groundwater flow in the deeper Paradox Basin until ~1 Ma by ^{81}Kr dating (Kim et al., 2022). Therefore, a more likely scenario is that the accelerated lowering of the eustatic sea level during the MPT induced changes in groundwater dynamics and water-rock interactions in the river basins and activated the drainage reorganization of the modern big rivers, including the Yellow River and Yangtze River.

In fact, a similar spillover of the paleo-Xigeda Lake in Eastern Tibet was also confirmed during the early Pleistocene by zircon U-Pb age spectra from the Pliocene-early Pleistocene Xigeda Formation and modern river sands (Zhao et al., 2021). The earliest terraces developed along the Three Gorges have been dated at ~1.16 and ~1.13 Ma in the middle reaches of the Yangtze River, and the Dadu River, respectively (Li et al., 2001; Zhao et al., 2013). Therefore, an early Pleistocene accelerated incision occurred both in the Yellow River and the Yangtze River, which was induced by the accelerated lowering of the eustatic sea level during the MPT. And the role of landscape evolution over the last few million years on the extent of recent subsurface flow systems and water-rock interaction could be evaluated by paleogroundwater studies.

5. Conclusions

Hydrochemical and isotope data were combined with ^{81}Kr and ^{36}Cl chronometers in a systematic data framework to improve our understanding of the past groundwater dynamics and water-rock interactions of the Weihe Basin. Two marked groups were divided by correcting ^{36}Cl ages with ^{81}Kr: one group with groundwater ages in the range of

350–813 ka (Cluster A) exhibits dead Cl dissolution and large positive $\delta^{18}O$ shifts, and the other group with ages >1.0 Ma (Cluster B) with negligible dead Cl dissolution and small $\delta^{18}O$ shifts.

The evolution of the groundwater and its age information revealed the change of the flow system in the Weihe Basin and constrains the birth time of the modern Yellow River. Since the MPT, the excavation of the Ancient Sanmen Lake and the accentuated incision of the Wei River induced groundwater recharge on both sides, from the Qinling Mountains in the south and the Beishan Mountains. The intense interaction between meteoric-originated groundwater and rock in the aquifers leads to an obvious oxygen-isotope shift and dead Cl dissolution for Cluster A. These waters flowed from north or south to the basin center, mixing with old groundwater (Cluster B) in the basin center with an eastward groundwater direction with discharge to the Ancient Sanmen Lake in the past.

CRediT authorship contribution statement

Jie Li: Writing – review & editing, Writing – original draft, Resources, Methodology, Data curation. **Zhonghe Pang:** Supervision, Conceptualization, Funding acquisition, Project administration, Resources, Writing – review & editing. **Yulian Liu:** Data curation. **Shuiming Hu:** Data curation. **Wei Jiang:** Data curation, Supervision, Validation, Writing – review & editing. **Lijun Tian:** Data curation. **Guomin Yang:** Data curation. **Ying Jiang:** Data curation. **Xuan Jiao:** Data curation. **Jiao Tian:** Investigation.

Declaration of Competing Interest

The authors declare that they have no known competing financial interests or personal relationships that could have appeared to influence the work reported in this paper.

Data availability

We have shared my data in attachment.

Acknowledgements

This work was supported by the Innovation Program for Quantum Science and Technology (2021ZD0303100), the National Natural Science Foundation of China (grant 42377058, 41602276, 41727901), the National Key Research and Development Program of China (2016YFA0302200) and International Atomic Energy Agency (RCA RAS7035). Sincere appreciation is given to the staff members of Sinopec Green Energy Geothermal Development Co. for help during field work.

Supplementarerials

Supplementary material associated with this article can be found, in the online version, at doi:10.1016/j.epsl.2023.118425.

References

Alley, W.M., Healy, R.W., Labaugh, J.W., Reilly, T.E., 2002. Hydrology-Flow and storage in groundwater systems. Science 296, 1985–1990. https://doi.org/10.1126/science.1067123.

Bentley, H.W., Phillips, F.M., Davis, S.N., 1986. Chlorine-36 in the terrestrial environment. In: Fritz, P., Fontes, J.-C. (Eds.), Handbook of Environmental Isotope Geochemistry, 2. Elsevier, Amsterdam, pp. 427–480. https://doi.org/10.1016/B978-0-444-42225-5.50015-2.

Bethke, C.M., Marshak, S., 1990. Brine migrations across North America-The plate tectonics of groundwater. Annu. Rev. Earth Planet. Sci 18 (1), 287–315. https://doi.org/10.1146/annurev.ea.18.050190.001443.

Clark, I., Fritz, P., 1997. Environmental Isotopes in Hydrogeology. Boca Raton, Lewis.

Ding, Z.L., Yang, S.L., 2000. C3/C4 vegetation evolution over the last 7.0 Myr in the Chinese Loess Plateau: evidence from pedogenic carbonate ^{13}C. Palaeogeogr. Palaeoclimatol. Palaeoecol 160, 291–299. https://doi.org/10.1016/S0031-0182(00)00076-6.

Davis, S.N., Moysey, S., Cecil, D.L., Zreda, M., 2003. Chlorine-36 in groundwater of the United States: empirical data. Hydrogeol. J 11, 217–227. https://doi.org/10.1007/s10040-002-0232-6.

Fehn, U., Moran, J.E., Teng, R.T.D., Rao, U., 1994. Dating and tracing of fluids using ^{129}I and ^{36}Cl: results from geothermal fluids, oil field brines and formation waters. Nucl. Instrum. Method. Phys. Res. Sect. B: Beam Interact. Mater. Atom. 92 (1–4), 380–384.

Garven, G., 1989. A hydrogeologic model for the formation of the giant oil sands deposits of the Western Canada sedimentary basin. Am. J. Sci 289 (2), 105–166. https://doi.org/10.1029/JB094iB02p01977.

Gerber, C., Vaikmäe, R., Aeschbach, W., Babre, A., Jiang, W., Leuenberger, M., Lu, Z.T., Mokrik, R., Müller, P., Raidla, V., Saks, T., Waber, H.N., Weissbach, T., Zappala, J.C., Purtschert, R., 2017. Using ^{81}Kr and noble gases to characterize and date groundwater and brines in the Baltic Artesian Basin on the one-million-year timescale. Geochim. Cosmochim. Acta 205, 187–210. https://doi.org/10.1016/j.gca.2017.01.033.

Giggenbach, W., 1988. Geothermal solute equilibria.derivation of Na-K-Mg-Ca geoindicators. Geochim. Cosmochim. Acta 52 (12), 2749–2765.

He, D., 2015. Isotopic and Hydrogeochemical Evidence of Remaining Sedimentary Water in the Deep Geothermal Reservoir of Guanzhong Basin. Master thesis. Chang'an University.

Horita, J., 2005. Isotopes in the Water Cycle: past, Present and Future of a Developing Science. Saline Waters 271–287.

Hu, Z., Li, M., Dong, Z., Guo, L., Bridgland, D., Pan, B., Liu, X., 2019. Fluvial entrenchment and integration of the Sanmen Gorge, the Lower Yellow River. Glob. Planet Change 178, 129–138. https://doi.org/10.1016/j.gloplacha.2019.04.010.

Jiang, W., Hu, S.M., Lu, Z.T., Ritterbusch, F., Yang, G.M., 2020. Latest development of radiokrypton dating-A tool to find and study paleogroundwater. Quatern. Int. 547, 166–171. https://doi.org/10.1016/j.quaint.2019.04.025.

Kim, J., Ferguson, G., Person, M., Jiang, W., Lu, Z.T., Ritterbusch, F., Yang, G.M., Tyne, R., Bailey, L., Ballentine, C., Reiners, P., McIntosh, J., 2022. Kypton-81 dating constrains timing of deep groundwater flow activation. Geophys. Res. Lett 49, e2021GL097618. https://doi.org/10.1029/2021GL097618.

Kong, P., Jia, J., Zheng, Y., 2014. Time constraints for the Yellow River traversing the Sanmen Gorge. Geochem. Geophys. Geosyst. 15, 395–407. https://doi.org/10.1002/2013GC004912.

Lazear, G., Karlstrom, K., Aslan, A., Kelley, S., 2013. Denudation and flexural isostatic response of the Colorado Plateau and southern Rocky Mountains region since 10 Ma. Geosphere 9 (4), 792–814. https://doi.org/10.1130/GES00836.1.

Lehmann, B., Davis, S., Fabryka-Martin, J., 1993. Atmospheric and subsurface sources of stable and radioactive nuclides used for groundwater dating. Water Resour. Res. 29, 2027–2040.

Lehmann, B.E., Love, A., Purtschert, R., Collon, P., Loosli, H.H., Kutschera, W., Beyerle, U., Aeschbach-Hertig, W., Kipfer, R., Frape, S.K., Herczeg, A., Moran, J., Tolstikhin, I.N., Gröning, M., 2003. A comparison of groundwater dating with ^{81}Kr, ^{36}Cl and ^{4}He in four wells of the Great Artesian Basin, Australia. Earth Planet. Sci. Lett 211, 237–250. https://doi.org/10.1016/S0012-821X(03)00206-1.

Lin, A., Yang, Z., Sun, Z., Yang, T., 2001. How and when did the Yellow River develop its square bend? Geology 29 (10), 951–954, 10.1130/0091-7613(2001)029<0951:HAWDTY>2.0.CO;2.

Li, J., Pang, Z., Yang, G.M., Tian, J., Tong, A.L., Zhang, X.Y., Hu, S.M., 2017. Million-year-old groundwater revealed by krypton-81 dating in Weihe Basin. Chin. Sci. Bulll 62, 1181–1184. https://doi.org/10.1016/j.scib.2017.08.009.

Li, J., Liu, Y., Dai, W., Li, J., Yang, P., Tian, L., Yu, S., Zuo, R., Zhai, Y., Song, W., Yang, F., Zhou, R., Wang, S., 2023. Nitrate attenuation with rising groundwater levels: an integrated assessment using isotope tracers and microbial signatures. J. Hydrol. 624 (2), 129911 https://doi.org/10.1016/j.jhydrol. 2023.129911.

Li, J.J., Xie, S.Y., Kuang, M.S., 2001. Geomorphic evolution of the Yangtze Gorges and the time of their formation. Geomorphology 41, 125–135. https://doi.org/10.1016/S0169-555X(01)00110-6.

Liu, J., Zhang, P., Lease, R.O., Zheng, D., Wan, J., Wang, W., Zhang, H., 2013. Eocene onset and late Miocene acceleration of Cenozoic intracontinental extension in the North Qinling range-Weihe graben: insights from apatite fission track thermochronology. Tectonophysics 584, 281–296. https://doi.org/10.1016/j.tecto.2012.01.025.

Liu, J., Wang, P., Chen, X.Q., Shi, W., Song, L.J., Hu, J.M., 2022. The changes in drainage systems of Weihe Basin and Sanmenxia Basin since late Pliocene give new insights into the evolution of the Yellow River. Front. Earth Sci. 9, 820674 https://doi.org/10.3389/feart.2021.820674.

Luo, L., Pang, Z., Liu, J., Hu, S., Rao, S., Li, Y., Lu, L., 2017. Determining the recharge sources and circulation depth of thermal waters in Xianyang geothermal field in Weihe Basin: the controlling role of Weibei Fault. Geothermics 69, 55–64. https://doi.org/10.1016/j.geothermics.2017.04.006.

Luo, L., Zhu, X., He, C., Mao, X., Xu, Z., Wang, X., Zhu, X., 2019. Study on the genesis of geothermal fluid in Xianyang geothermal field. Geolog. Rev. 65, 1422–1430.

Lu, Z.T., Schlosser, P., Smethie, W.M., Sturchio, N.C., Fischer, T.P., Kennedy, B.M., Purtschert, R., Severinghaus, J.P., Solomon, D.K., Tanhua, T., Yokochi, R., 2014. Tracer applications of noble gas radionuclides in the geosciences. Earth-Sci. Rev. 138, 196–214. https://doi.org/10.1016/j.earscirev.2013.09.002.

Matsumoto, T., Chen, Z., Wei, W., Yang, G.M., Hu, S.M., Zhang, X., 2018. Application of combined ^{81}Kr and ^{4}He chronometers to the dating of old groundwater in a tectonically active region of the North China Plain. Earth Planet. Sci. Let.t 493, 208–217. https://doi.org/10.1016/j.epsl.2018.04.042.

Matsumoto, T., Zouari, K., Trabelsi, R., Hillegonds, D., Jiang, W., Lu, Z.T., Mueller, P., Zappala, J.C., Araguas, L.J., Romeo, N., Agoun, A., 2020. Krypton-81 dating of the

deep Continental Intercalaire aquifer with implications for chlorine-36 dating. Earth Planet. Sci. Lett. 535, 116120 https://doi.org/10.1016/j.epsl.2020.116120.
Ma, Z., Zhang, X.D.H., 2016. A study of ^{36}Cl age for the deep geothermal water in the Weihe basin (in Chinese). Hydrogeol. Eng. Geol 43, 157–163.
Meng, Q.R., 2017. Origin of the Qinling Mountains (in Chinese). Scientia Sinica Terrae 47, 412–420.
Mercier, J.L., Vergely, P., Zhang, Y.Q., Hou, M.J., Bellier, O., Wang, Y.M., 2013. Structural records of the Late Cretaceous—Cenozoic extension in Eastern China and the kinematics of the Southern Tan-Lu and Qinling Fault Zone (Anhui and Shaanxi provinces, PR China). Tectonophysics 582, 50–75. https://doi.org/10.1016/j.tecto.2012.09.015.
Miao, Y., Fang, X., Sun, J., Xiao, W.J., Yang, Y.H., Wang, X.L., Farnsworth, A., Huang, K. Y., Ren, Y.L., Wu, F.L., Qiao, Q.Q., Zhang, W.L., Meng, Q.Q., Yan, X.L., Zheng, Z., Song, C.H., Utescher, T., 2022. A new biologic paleoaltimetry indicating Late Miocene rapid uplift of northern Tibet Plateau. Science 378 (6624), 1074–1079. https://doi.org/10.1126/science.abo2475.
Moysey, S., Davis, S.N., Zreda, M., Cecil, L.D., 2003. The distribution of meteoric ^{36}Cl/Cl in the United States: a comparison of models. Hydrogeol. J. 11, 615–627. https://doi.org/10.1007/s10040-003-0287-z.
Murray, K.E., Reiners, P.W., Thomson, S.N., Robert, X., Whipple, K.X., 2019. The thermochronologic record of erosion and magmatism in the Canyonlands region of the Colorado Plateau. Am. J. Sci. 319 (5), 339–380. https://doi.org/10.2475/05.2019.01.
Pan, B., Wang, J., Gao, H., Guan, Q., Wang, Y., Su, H., Li, J., 2005. Paleomagnetic dating of the topmost terrace in Kouma, Henan and its indication to the Yellow River's running through Sanmen Gorges. Chin. Sci. Bull. 50, 657–664. https://doi.org/10.1360/03wd0290.
Pang, Z., Reed, M.H., 1998. Theoretical chemical thermometry on geothermal waters: problems and methods. Geochim. Cosmochim. Acta 62 (6), 1083–1091.
Park, J., Bethke, C.M., Torgersen, T., Johnson, T.M., 2002. Transport modeling applied to the interpretation of groundwater ^{36}Cl age. Water Resour. Res. 38 https://doi.org/10.1029/2001WR000399, 1-1-1-15.
Patterson, L.J., Sturchio, N.C., Kennedy, B.M., van Soest, M.C., Sultan, M.I., Lu, Z.T., Lehmann, B.E., Purtschert, R., El Kaliouby, B., Dawood, Y., Abdallah, A.M., 2005. Cosmogenic, radiogenic, and stable isotopic constraints on groundwater resi-dence time in the Nubian Aquifer, Western Desert of Egypt. Geochem. Geophys. Geosyst. 6 (1) https://doi.org/10.1029/2004GC000779. Q01005.
Phillips, F.M., 2000. Chlorine-36. In: Cook, P.G., Herczeg, A.L. (Eds.), Environmental Tracers in Subsurface Hydrology. Kluwer Academic Publishers, pp. 299–348. https://doi.org/10.1029/2001WR000399.
Phillips, F.M., 2013. Chlorine-36 dating of old groundwater. Isotope Method. Dating Old Groundwater 125–152.
Qin, D., Turner, J.V., Pang, Z., 2005. Hydrogeochemistry and groundwater circulation in the Weihe Basin, China. Geothermics 34, 471–494.
Sherif, M.I., Sultan, M., Sturchio, N.C., 2019. Chlorine isotopes as tracers of solute origin and age of groundwaters from the Eastern Desert of Egypt. Earth Planet. Sci. Lett. 510, 37–44. https://doi.org/10.1016/j.epsl.2018.12.035.
Sturchio, N.C., Du, X., Purtschert, R., Lehmann, B.E., Sultan, M., Patterson, L.J., Lu, Z.T., Müller, P., Bigler, T., Bailey, K., O'Connor, T.P., Young, L., Lorenzo, R., Becker, R., El Alfy, Z., El Kaliouby, B., Dawood, Y., Abdallah, A.M.A., 2004. One million-year-old groundwater in the Sahara revealed by krypton-81 and chlorine-36. Geophys. Res. Lett 31. https://doi.org/10.1029/2003GL019234 n/a-n/a.
Wang, X., Hu, G., Saito, Y., Ni, G., Hu, H., Yu, Z., Chen, J., Wang, M., Yuan, X., Wang, L., Hu, Z., Nie, J., Pan, B., 2022. Did the modern Yellow River form at the Mid-Pleistocene transition? Sci. Bull. 67, 1603–1610. https://doi.org/10.1016/j.scib.2022.06.003.
Yang, J., Gao, S., Chen, C., Tang, Y., Yuan, H., Gong, H., Xie, S., Wang, J., 2009. Episodic crustal growth of North China as revealed by U-Pb age and Hf isotopes of detrital zircons from modern rivers. Geochim. Cosmochim. Acta 73 (9), 2660–2673. https://doi.org/10.1016/j.gca.2009.02.007.
Yager, R.M., McCoy, K.J., Voss, C.I., Sanford, W.E., Winston, R.B., 2017. The role of uplift and erosion in the persistence of saline groundwater in the shallow subsurface. Geophys. Res. Lett. 44 (8), 3672–3681. https://doi.org/10.1002/2017GL072980.
Yechieli, Y., Yokochi, R., Zilberbrand, M., Lu, Z.T., Purtschert, R., Sueltenfuss, J., Jiang, W., Zappala, J., Mueller, P., Bernier, R., Avrahamov, N., Adar, E., Talhami, F., Livshitz, Y., Burg, A., 2019. Recent seawater intrusion into deep aquifer determined by the radioactive noble-gas isotopes ^{81}Kr and ^{39}Ar. Earth Planet. Sci. Lett. 507, 21–29. https://doi.org/10.1016/j.epsl.2018.11.028.
Yokochi, R., Ram, R., Zappala, J.C., Jiang, W., Adar, E., Bernier, R., Burg, A., Dayan, U., Lu, Z.T., Mueller, P., Purtschert, R., Yechieli, Y., 2019. Radiokrypton unveils dual moisture sources of a deep desert aquifer. Proc. Natl. Acad. Sci. 116 (33), 16222–16227. https://doi.org/10.1073/pnas.1904260116.
Zappala, J.C., Baggenstos, D., Gerber, C., Jiang, W., Kennedy, B.M., Lu, Z.T., Visser, A., 2020. Atmospheric ^{81}Kr as an integrator of cosmic-ray flux on the hundred-thousand-year time scale. Geophys. Res. Lett. 47 (3) https://doi.org/10.1029/2019GL086381 e2019GL086381.
Zhang, W., Li, Y., Zhao, F., Han, W., Li, Y., Wang, Y., Holland, G., Zhou, Z., 2019. Using noble gases to trace groundwater evolution and assess helium accumulation in Weihe Basin, central China. Geochim. Cosmochim. Acta 251, 229–246. https://doi.org/10.1016/j.gca.2019.02.024.
Zhang, H., Lu, H.Y., Zhou, Y.L., Cui, Y.Y., He, J., Lv, H.Z., Wang, K.X., Wang, X.Y., 2021. Heavy mineral assemblages and UePb detrital zircon geochronology of sediments from the Weihe and Sanmen Basins: new insights into the Pliocene-Pleistocene evolution of the Yellow River. Palaeogeogr. Palaeoclimatol. Palaeoecol.: Int. J. Geo-Sci. 562, 110072.
Zhao, Z.J., Liu, Y., Chen, Y., Zhang, M.H., Shu, Q., Li, C.L., Li, P., 2013. Quaternary fluvial incision rates of the Western Sichuan Plateau inferred from ESR chronology. J. Lanzhou Univer. (Nat. Sci.) 49, 160–167.
Zhao, X.D., Zhang, H.P., Tao, Y.L., Wang, Y., Pang, J.Z., Ma, Y., Zhang, J.W., Ma, Z.F., Xiong, J.G., 2021. Pliocene to Early Pleistocene drainage reorganization in eastern Tibet inferred from detrital zircons. Geophys. Res. Lett 48. https://doi.org/10.1029/2021GL094563 e2021GL094563.
Jiang, W., Bailey, K., Lu, Z.T., Mueller, P., O'Connor, T.P., Cheng, C.F., Hu, S.M., Purtschert, R., Sturchio, N.C., Sun, Y.R., Williams, W.D., Yang, G.M., 2012. An atom counter for measuring ^{81}Kr and ^{85}Kr in environmental samples. Geochim. Cosmochim. Acta 91, 1–6. https://doi.org/10.1016/j.gca.2012.05.019.